PAPER

Check for updates

Degradation of organic pollutants through activating bisulfite with lanthanum ferrite-loaded biomass carbon

Xiangyu Meng,[a] Yao Li,[a] Yiqing Liu, [ID] *[a] Runyu Zhou,[b] Yongsheng Fu[a] and Junmin Chen[a]

The removal of methylene blue (MB) in water is a challenging task due to its toxicity, carcinogenicity and resistance to biodegradation. Accordingly, a novel composite catalyst (BC@LF) was prepared by loading lanthanum ferrite ($LaFeO_3$) on biomass carbon (BC) to activate bisulfite (BS) for methylene MB removal in this study. Characterization *via* scanning electron microscopy (SEM), X-ray diffraction (XRD) and Fourier transform infrared spectroscopy (FTIR) indicated that $LaFeO_3$ was successfully loaded on BC. X-ray photoelectron spectroscopy (XPS) analysis suggested that $\equiv$Fe(III) was the main active site for BS activation. It was found that 99.4% MB was removed within 60 min in BC@LF/BS system. Sulfate radical ($SO_4^{\bullet-}$) and hydroxyl radicals (HO$^{\bullet}$) were proved to be responsible for MB removal in the BC@LF/BS system and $SO_5^{\bullet-}$ might also be involved in MB removal. The degradation efficiency of MB in the BC@LF/BS system decreased with increasing pH, while the adsorption efficiency of BC@LF for MB improved with increasing pH. Additionally, BC@LF exhibited good reusability for BS activation in successive uses. The BC@LF/BS system exhibited favorable removal effect for various organic compounds, indicating that it has good applicability in the treatment of organic wastewater.

1 Introduction

In recent years, organic pollutants have gained significant attention in academic research. Among various organic pollutants, organic dye wastewater has emerged as a core environmental concern due to its extensive discharge, high toxicity, intense color and complicated composition.[1] As a representative organic dye, methylene blue (MB) is widely applied in the printing and dyeing industry. However, its toxic and carcinogenic nature, along with its strong resistance to biodegradation, poses substantial challenges for wastewater treatment.[2] Therefore, the primary objective of this study was to explore an effective method for the removal of MB, aiming to address the pressing issue of organic dye pollution.

Advanced oxidation processes (AOPs) are efficient techniques for the degradation of refractory contaminants, because they can produce highly reactive oxygen species (ROS), such as the hydroxyl radical (HO$^{\bullet}$), sulfate radical ($SO_4^{\bullet-}$), superoxide radical ($O_2^{\bullet-}$) and singlet oxygen ($1O_2$).[3] Since $SO_4^{\bullet-}$ possesses a higher redox potential (2.5–3.1 V *vs.* HO$^{\bullet}$: 2.7 V) and a longer half-life than HO$^{\bullet}$, $SO_4^{\bullet-}$-based AOPs exhibit a higher removal efficiency toward various organic pollutants.[4,5] Persulfates (PS, *e.g.*, peroxydisulfate (PDS) and peroxymonosulfate (PMS)) are

traditional precursors of $SO_4^{\bullet-}$, and UV radiation, heat as well as transition metal are the common activators for them. Among these activators, transition metal is regarded as the most cost-effective one due to its highly catalytic performance and easy availability. However, once these transition metal ions are oxidized, they will be ineffective for PS activation. Therefore, to improve the regeneration of active transition metal ions, developing a cycle system that converts the transition metal ions from high valence state to low valence state, is of great significance for the practical application of $SO_4^{\bullet-}$-based AOPs. Bisulfite (BS) is widely used as reductant, dechlorination and food preservative due to its reductive property, which has the potential to reduce the high-valent transition metal ions. For instance, BS has been successfully used to reduce Fe(III) to Fe(II).[6]

Except reduction, BS is also used as a precursor of $SO_4^{\bullet-}$, which has attracted extensive attention in AOPs.[7–9] Currently, UV light and transition metals (*e.g.*, Fe, Co, Mn and Cr)[9–13] have been reported to be able to effectively activate BS producing ROS. However, UV light requires high energy consumption.[14] Among these transition metals, Fe is a commonly used and efficient BS catalyst because Co, Mn and Cr have a potential risk of secondary pollution.[15,16] Nevertheless, in homogeneous Fe-catalyzed BS systems, strongly acidic condition is needed. Fortunately, heterogeneous materials tend to have a wide range of working pH in AOPs.[17,18] Therefore, developing heterogeneous Fe-based materials provides an ideal solution for

[a]Faculty of Geosciences and Environmental Engineering, Southwest Jiaotong University, Chengdu 611756, China. E-mail: liuyq@swjtu.edu.cn

[b]Zhejiang Development & Planning Institute, Hangzhou, 310012, China

overcoming the above limitation in BS activation. Among various iron-based porous materials, the catalyst with perovskite configuration may become a magnetic material with good catalytic property,[19] making it an ideal candidate for BS catalysis. Perovskite, a complex oxide in the shape of a cube or octahedron, exhibits better electrochemical and redox properties due to its internal cations and abundant oxygen vacancy (OV).[19] Meanwhile, perovskite can be used over a wide pH range and is easy to be recycled. Therefore, it may be a promising activator for peroxides in AOPs, which has been successfully applied in the activation of PDS and PMS.[20,21] The molecular formula of perovskite is ABO_3, in which A is usually rare earth or alkaline earth element and B is usually transition metal element. Lanthanum ferrite ($LaFeO_3$) with a classical perovskite structure seems to be a potential heterogeneous catalyst for peroxides, based on excellent structural stability and environment-friendly property. Practically, $LaFeO_3$ is the most common catalyst used in the perovskites-activated AOPs.[22–24] For example, $LaFeO_3$ has been successfully applied in the activation of H_2O_2, PDS and PMS for the degradation of sulfamethoxazole (SMX), 4-chlorophenol and diclofenac (DCF), respectively. However, $LaFeO_3$ also exhibits some drawbacks in above cases, such as limited specific surface area and low catalytic efficiency. Hence, some approaches are required to be taken for solving the above shortcomings of $LaFeO_3$.

Fortunately, loading $LaFeO_3$ on a material with large specific surface area may enhance its dispersibility and subsequent catalytic efficiency. Recently, carbon-based materials are commonly used as a carrier of catalysts, due to their abundant porous structure,[25] large specific surface area[26] and rich oxygen-containing active groups.[27] Peanut shell is considered as a promising preparation precursor of biomass carbon (BC) due to its natural abundance, low cost and nontoxicity.[28] Therefore, the novel composite catalyst $BC@LaFeO_3$ (BC@LF), which was formed by $LaFeO_3$ loading in BC, might have exhibited improved catalytic activity. Currently, the report about loading $LaFeO_3$ to BC is limited. Yang et al.[29] successfully developed an efficient, economical and environment-friendly composite material by loading $LaFeO_3$ onto straw biochar to adsorb high-concentration phosphate wastewater. Meanwhile, Chen et al.[30] utilized lignin biochar loaded $LaFeO_3$ to catalyze H_2O_2 under visible light irradiation for the degradation of ofloxacin. To the best of our knowledge, BC@LF was firstly applied to activate BS in this work. MB was selected as the target contaminant to evaluate the catalytic efficiency of BC@LF on BS. Table 1 shows the previous studies on the activation of BS for MB degradation.

The primary aims of this study were to: (1) examine the feasibility and mechanism of BS activation by BC@LF; (2) determine the primary reactive species responsible for MB removal in BC@LF/BS system; and (3) investigate the reusability and stability of BC@LF for BS activation.

2 Materials and methods

2.1. Reagents

MB, RhB, orange G (OG), DCF, SMX, ofloxacin (OFX), *tert*-butyl alcohol (TBA), lanthanum nitrate hexahydrate ($La(NO_3)_3 \cdot 6H_2O$), BS and 5,5′-dithiobis (2-nitrozoicacid) (DTNB) were purchased from Aladdin Reagent Company, China. Methanol (MeOH), citric acid (CA), potassium tellurite (K_2TeO_3), iron nitrate nonahydrate ($Fe(NO_3)_3 \cdot 9H_2O$), H_2SO_4, NaOH, NaCl, $NaNO_3$, $NaHCO_3$, Na_2SO_4, $Na_2S_2O_3$, $FeCl_3$, $CuCl_2$, $MgCl_2$ and $CaCl_2$ were all analytical grade and purchased from Chengdu Kelong Chemical Reagent Co., Ltd, China. Deionized water was used in all experiments.

2.2. Synthesis of BC@LF

Firstly, the peanut shell powder was prepared as follows. The peanut shell was washed with deionized water to remove the dirt on its surface, and then dried in an oven at 65 °C for 24 h. Subsequently, the dried peanut shell was crushed and screened with 120-mesh sieve. Finally, the obtained peanut shell powder was washed with deionized water and dried at 65 °C for 24 h for further use. Secondly, BC@LF was synthesized through a sol–gel method as follows. 0.01 mol of ($La(NO_3)_3 \cdot 6H_2O$) and 0.01 mol of $Fe(NO_3)_3 \cdot 9H_2O$ were dissolved in 40 mL deionized water, respectively, and then, 0.03 mol CA was added into the mixed solution. Next, 6 g peanut shell powder was added into the above solution and mixed for 30 min. The aforementioned solution was mechanically stirred in a thermostatic bath at 70 °C for 10 min and sonicated for 10 min, which was repeated for 5 times. Subsequently, the pretreated solution was heated at 70 °C until it became a yellow-brown sol, and then dried at 105 °C for 24 h to obtain a yellow-brown gel. Finally, the xerogel was ground into powder and heated in a muffle furnace at 600 °C for 2 h with a heating rate of 10 °C min^{-1}. After cooling down to room temperature, the obtained product was ground into powder for further use. Additionally, the $LaFeO_3$, Fe_2O_3, La_2O_3, $BC@Fe_2O_3$, $BC@La_2O_3$ and BC were synthesized *via* the same way without adding the corresponding materials.

2.3. Experimental procedure

The 250 mL beaker was used as the reaction container with constant mechanical stirring at 25 °C. At first, predetermined concentrations of MB and BS were added. Then, the initial pH of reaction solution was adjusted to the designated value by adding 0.5 M of H_2SO_4 and 0.5 M of NaOH. Finally, the reaction was initiated with the addition of the catalyst. At determined time intervals, 1 mL sample was taken out, then quenched with 1 mL 50 mM of $Na_2S_2O_3$, and filtered through 0.22 μm membrane for further analysis. The used BC@LF was recovered by magnetic separation and washed with deionized water for

Table 1 Comparison of the effectiveness with related catalysts

Catalyst	BS dosage (mM)	MB dosage (mg L^{-1})	Removal ratio (%)
CoO[31]	19	30	99.4
Co_3O_4/CoO[32]	19	30	90.7
Fe-Mn$_X$ oxides[33]	10	30	81.0–92.0
Red mud@$LaFeO_3$ [34]	10	10–80	72.4–100.0
BC@LF (this work)	5	15	99.4

three times after each round and dried in vacuum at 60 °C for 24 h. Subsequently, the reusability experiments were conducted under the same conditions. All the experiments were performed at least twice and the averages are shown in the figures.

2.4. Analysis

The surface morphology and element mapping of the materials were revealed by a scanning electron microscope (SEM) (Carl Zeiss, Gemini 300) coupled with an energy diffraction spectrum (EDS) (OXFORD, Xplore). X-ray photoelectron spectroscope (XPS) (Thermo Scientific, K-Alpha) was used to investigate the elemental composition and valence states of the samples. The X-ray diffraction (XRD) patterns were collected by an X-ray diffractometer (Panalytical, Ultima IV) to determine the surface crystallization status of the samples. Brunauer–Emmett–Teller (BET) method was used to determine the specific surface area of the samples by a physisorption analyzer (Micromeritics, ASAP2460). The Fourier transformation infrared spectroscopy (FTIR) (Thermo Scientific, Nicolet IS50) was used to investigate the functional groups and chemical bonds of the samples. The inductive coupling plasma mass-spectrometric (ICP-MS) (Agilent 7700s (MS)) was used to measure the leaching of metal element. The concentration of MB was determined using an UV-Vis spectrophotometer (UNICO, UV4802) at the maximum absorption wavelength of 665 nm. The solution pH was monitored using a pH meter (Leici, PHS-3C). The removal ratio of MB was calculated *via* eqn (1), and the standard deviation of replicate experiments for the samples was calculated *via* eqn (2)

$$\eta_D = \left(1 - \frac{C}{C_0}\right) \times 100\% \tag{1}$$

$$s = \sqrt{\frac{\sum (x_i - \overline{x})^2}{n}} \tag{2}$$

where η_D is the removal ratio of MB; C_0 is initial concentration of MB; C is the concentration of MB at the sampling time; s is the sample standard deviation; x_i is the i-th data point; $\overline{x}$ is the mean of the sample data; n is the number of data points in the sample.

3 Results and discussion

3.1. Characterization of catalysts

3.1.1 SEM analysis. As shown in Fig. 1a, the morphology of BC exhibited a smooth lamellar structure. LaFeO$_3$ displayed many agglomerated spherical nanoparticles, as shown in Fig. 1b. However, in the SEM image of fresh BC@LF (Fig. 1c), the lamellar structure of BC was changed to a porous structure. This might be due to that there were large number of bubbles in the colloid during the assistance of ultrasonic wave process and the citric acid used as the complexing agent could be gasified during the calcination process.[35] Meanwhile, the morphology of particles on the surface of fresh BC@LF was similar with that of LaFeO$_3$ particles.[36] Therefore, many particles were observed in fresh BC@LF, indicating that LaFeO$_3$ was loaded on BC
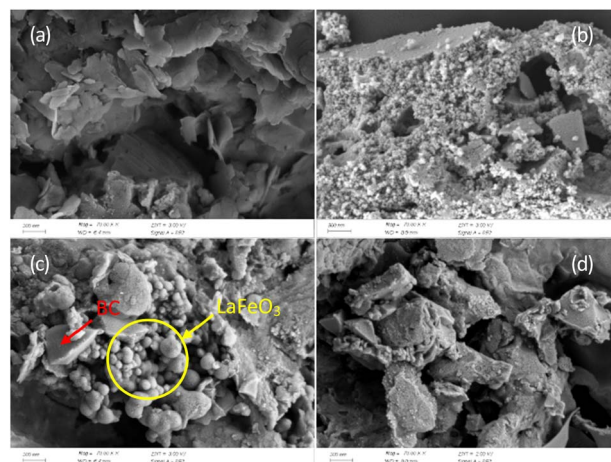

Fig. 1 SEM images of BC (a), LaFeO$_3$ (b), fresh BC@LF (c) and used BC@LF (d).

successfully. For comparison, the morphology of used BC@LF was also recorded in Fig. 1d. The original agglomerated particles disappeared in used BC@LF, which might be attributed to the consumption of LaFeO$_3$ during BS activation.

3.1.2 XRD analysis. Fig. 2 shows the XRD patterns of BC, LaFeO$_3$ and BC@LF. In the XRD pattern of BC, two strong peaks at 26.69° and 50.26° were the characteristic peaks of C, the peak at 26.69° suggests that the graphene sheets are stacked coherently in a narrow range,[37] and the peak at 50.26° is a characteristic feature of the honeycomb lattice structure formed by sp^2 hybridized carbon.[38,39] The diffraction peaks at 22.63°, 32.22°, 39.73°, 46.21°, 52.04°, 57.45°, 67.41° and 76.70° in the XRD pattern of LaFeO$_3$ were well assigned to the (100), (110), (111), (200), (210), (220), (221) and (310) crystal planes of LaFeO$_3$ (PDF#75-0439), respectively. In the XRD pattern of fresh BC@LF, both the characteristic peaks of LaFeO$_3$ and BC were observed, indicating that LaFeO$_3$ was successfully loaded on BC, which was in accordance with SEM results. In addition, the XRD
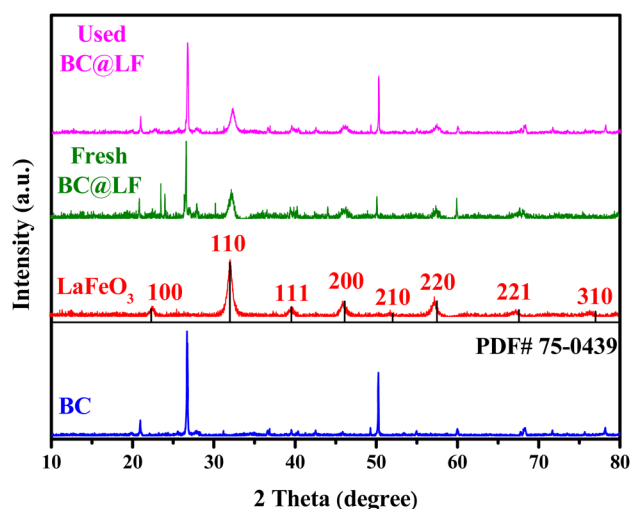

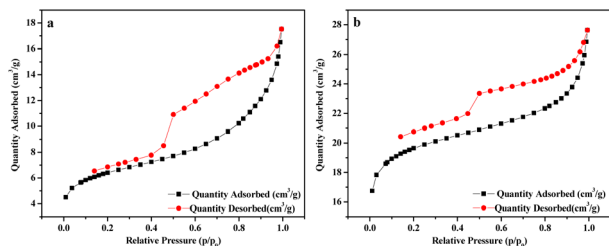Fig. 2 XRD patterns of LaFeO$_3$, fresh BC@LF, used BC@LF and BC.

Fig. 3 N$_2$ adsorption–desorption isotherm curves of BC (a) and BC@LF (b).

Fig. 5 FTIR spectra of BC, fresh BC@LF and used BC@LF.

pattern of used BC@LF had no significant changes, indicating that BC@LF might have a good stability.

3.1.3 BET analysis. The specific surface area and pore volume of BC and BC@LF were determined by BET analysis. As shown in Fig. 3, the N$_2$ adsorption/desorption isotherms of BC and BC@LF could be both fitted into type II isotherms, and the adsorption capacity increased rapidly when the relative pressure was low in the adsorption process.[40] The inflection point of the isotherm also indicated that the adsorption of monolayer was saturated.[40] A gradual curvature in the adsorption isotherm suggested a partial overlap between the monolayer coverage and the onset of multilayer adsorption. As the relative pressure (p/p_0) approached 1, the thickness of the adsorbed multilayer increased without any upper bound.[41] The specific surface area, pore size, and pore volume of BC and BC@LF were determined using the Barrett–Joyner–Halenda (BJH) method. As presented in Table 2, BC@LF exhibited a higher specific surface area and pore volume, but a smaller pore size than BC, because the loading of LaFeO$_3$ resulted in a significant reduction in mesopores on BC but a notable increase in micropores, as illustrated in Fig. 4. Therefore, the introduction of LaFeO$_3$ in BC could enlarge its specific surface area and pore volume, making

Table 2 Specific surface area and pore volume of BC and BC@LF

	Specific surface area	Pore size	Pore volume
BC	23.2045 m^2 g^{-1}	46.088 nm	0.026736 cm^3 g^{-1}
BC@LF	71.9031 m^2 g^{-1}	23.727 nm	0.042652 cm^3 g^{-1}

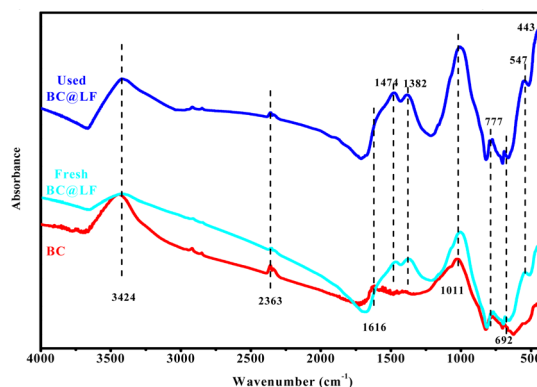Fig. 4 Pore size distribution of BC and BC@LF by BJH method.

BC@LF possessed a stronger adsorption capacity than BC, which was in accordance with the results of MB degradation by their adsorption.

3.1.4 FTIR analysis. Fig. 5 shows the FTIR spectra of BC and BC@LF. In the FTIR spectrum of BC, the main absorption peaks were assigned to the aromatic C–H bending (at 692 and 777 cm^{-1}),[42] C–O stretching vibration in the conjugated carboxyl (at 1011 cm^{-1}),[40] stretching vibration of C=O (at 1616 and 2363 cm^{-1})[43,44] and bending vibration and stretching vibration of absorbing water (at 3424 cm^{-1}).[45] In the FTIR spectrum of BC@LF, the absorption peaks at 443 and 547 cm^{-1} were characteristic peaks of O–Fe–O and Fe–O, respectively.[44,46] The absorption peaks at 1382 and 1474 cm^{-1} were characteristic peaks of La–O,[47,48] which further proved that LaFeO$_3$ was successfully loaded on BC to form BC@LF. Additionally, the characteristic peaks of O–Fe–O, Fe–O and La–O were also present in the used BC@LF, indicating that the functional groups of used BC@LF exhibited little change.

3.1.5 XPS analysis. The XPS survey spectrum of fresh BC@LF is shown in Fig. 6a. As expected, C, O, Fe and La signals were clearly detected in the survey spectrum. In the C 1s spectrum of fresh BC@LF, three peaks at 284.8, 286.0 and 288.5 eV could be assigned to C=C, C–O–C and O–C=O, respectively, as shown in Fig. 6b. Peaks at binding energies of 705.8, 710.4 and 711.8 eV in Fe 2p spectrum (Fig. 6c) could be assigned to Fe 2p$_{3/2}$ of ≡Fe(II), ≡Fe(III) and ≡Fe(IV), respectively, and peaks at 719.6, 719.6 and 725.4 eV were the characteristics of ≡Fe(II), ≡Fe(III) and ≡Fe(IV) in Fe 2p$_{1/2}$, respectively.[49,50] The peak intensity indicated that Fe mainly existed in the form of ≡Fe(III) and ≡Fe(IV) in BC@LF, while the presence of ≡Fe(II) was negligible. Besides, peaks at 835.2 and 851.9 eV in La 3d spectrum (Fig. 6d) were the characteristics of ≡La(III) in La 3d$_{5/2}$ and La 3d$_{3/2}$, respectively,[51] which indicated that La in fresh BC@LF existed in the form of ≡La(III).

For comparison, the XPS spectrum of used BC@LF was also recorded. In the survey spectrum of used BC@LF (Fig. 6a), strong signals of C, O, Fe and La could still be observed. In the C 1s spectrum of used BC@LF (Fig. 6b), the signal of C hardly changed. However, the peak intensity of relative components changed in the Fe 2p spectrum of used BC@LF (Fig. 6c). Correspondingly, the proportion of ≡Fe(II) and ≡Fe(III)
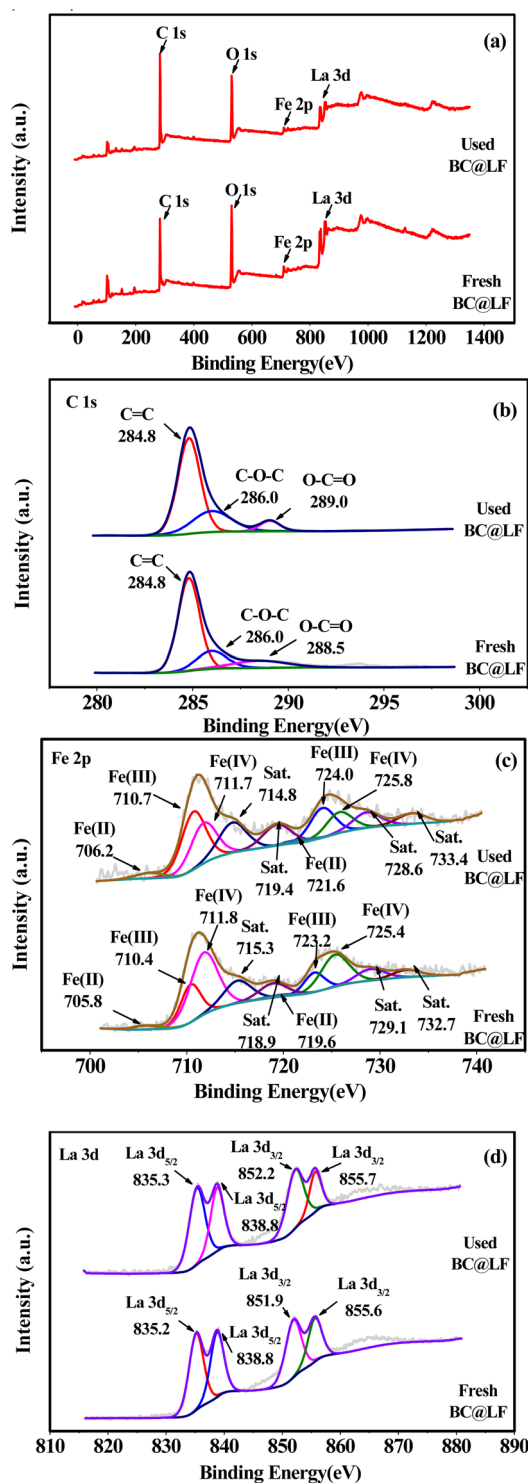
Fig. 6 XPS spectra of fresh and used BC@LF: survey spectra (a), C 1s (b), Fe 2p (c), La 3d (d).

increased but the ratio of ≡Fe(IV) decreased significantly in the used BC@LF. This result could be attributed to that ≡Fe(IV) and ≡Fe(III) were reduced to low valence states due to the strongly reductive ability of BS.[6,52,53] As presented in Fig. 6d, the signal of La 3d in used BC@LF hardly changed, indicating that La might not participate in the reaction.[54]

3.2. Removal of MB by BC@LF/BS

Fig. 7 shows the removal of MB in different systems. In BC alone system, 40.6% MB was removed within 60 min due to the excellent adsorption capacity of BC, while a negligible MB degradation was obtained in LaFeO₃ alone system, suggesting a low adsorption capacity of the prepared LaFeO₃. When LaFeO₃ was loaded on BC, the adsorption ability of BC might be enhanced based on the result that MB removal in BC@LF alone system was higher than that in BC alone system. Although MB was hardly removed in BS alone system, the combination of BC@LF and BS could induce 99.4% MB removal, which suggested that the prepared BC@LF could activate BS to produce reactive species degrading MB. To identify the active component for BS activation in BC@LF, the degradation of MB in BC/BS and LaFeO₃/BS systems were conducted. As presented in Fig. 1, the removal of MB in BC/BS system was similar with that in BC alone system, but 47.2% MB was degraded in LaFeO₃/BS system compared with negligible MB removal in LaFeO₃ alone and BS alone systems. These results indicated that BC was ineffective to catalyze BS and LaFeO₃ might be an active ingredient in BC@LF for BS activation.

3.3. BS activation mechanism by BC@LF

The above characterization results suggested that ≡Fe might be the active sites in BC@LF for BS activation to produce reactive radicals. According to the previous studies of BS activation systems,[53–58] oxysulfur radicals ($SO_3^{\bullet-}$, $SO_4^{\bullet-}$ and $SO_5^{\bullet-}$) and $HO^{\bullet}$ were the main radicals generated. Based on the above analysis, a possible BS activation mechanism was proposed in Fig. 8. Firstly, the surface ≡Fe(III) could accept an electron from BS to initiate the reaction producing $SO_3^{\bullet-}$ (eqn (3) and (4)). Meanwhile, ≡Fe(III) could be reduced to ≡Fe(II). Subsequently, $SO_4^{\bullet-}$, $SO_5^{\bullet-}$ and $HO^{\bullet}$ could be generated from $SO_3^{\bullet-}$ via chain reactions (eqn (5)–(11)). Besides, the formed ≡Fe(II) could also be oxidized to ≡Fe(III) (eqn (12)–(15)), constituting the redox cycle of ≡Fe(III)/≡Fe(II).

To further investigate the role of La in LaFeO₃, the MB removal in different systems were conducted. As shown in

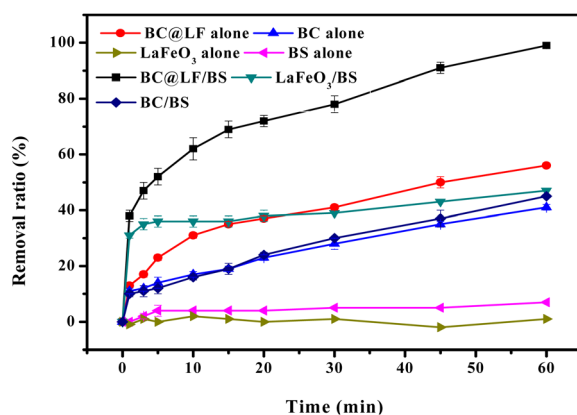Fig. 7 Removal of MB in different systems. Experimental conditions: $[MB]_0 = 15$ mg L^{-1}, $[BC@LF]_0 = [BC]_0 = [LaFeO_3]_0 = 3$ g L^{-1}, $[BS]_0 = 5$ mM, $T = 25$ °C, $pH_0 = 7$.
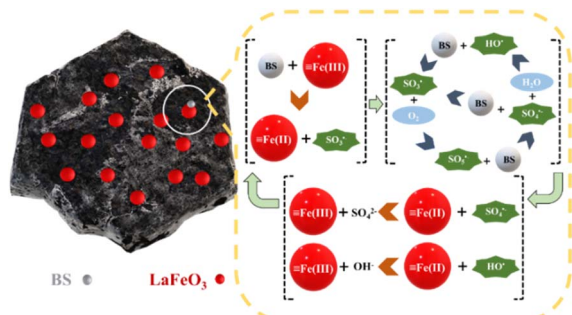
Fig. 8 Possible mechanism for BS activation by BC@LF.

Fig. 9, MB could not be removed efficiently in La$_2$O$_3$/BS and Fe$_2$O$_3$/BS systems, suggesting that La$_2$O$_3$ and Fe$_2$O$_3$ were ineffective for BS activation. Similarly, BC@La$_2$O$_3$ and BC@Fe$_2$O$_3$ were also ineffective for BS activation because the MB removal in BC@La$_2$O$_3$/BS and BC@Fe$_2$O$_3$/BS systems was similar with that in BC/BS system. However, BS could be activated by LaFeO$_3$ effectively, indicating that La and Fe coexisted in oxide could enhance the catalytic performance of this catalyst. This enhancement effect might be due to that the high oxygen-storage capacity (OSC) of La could generate more OV in LaFeO$_3$, promoting internal electron transfer.[35] Besides, the MB removal ratio in BC@La$_2$O$_3$/BS system was higher than that in BC@Fe$_2$O$_3$/BS system, because the large molecular structure of lanthanum oxide could improve the surface area and adsorption capacity of composite material.[36]

As stated above, SO$_3$$^{•−}$, SO$_4$$^{•−}$, SO$_5$$^{•−}$ and HO$^•$ might be produced in BC@LF/BS system. However, the role of SO$_3$$^{•−}$ in the degradation of organics could be negligible due to its weak oxidation potential and high reactivity toward O$_2$.[55] Therefore, in order to clarify the contribution of SO$_4$$^{•−}$, SO$_5$$^{•−}$ and HO$^•$ to MB removal, two radical scavengers (i.e., TBA and MeOH) were introduced in BC@LF/BS system. The rate constant of TBA with
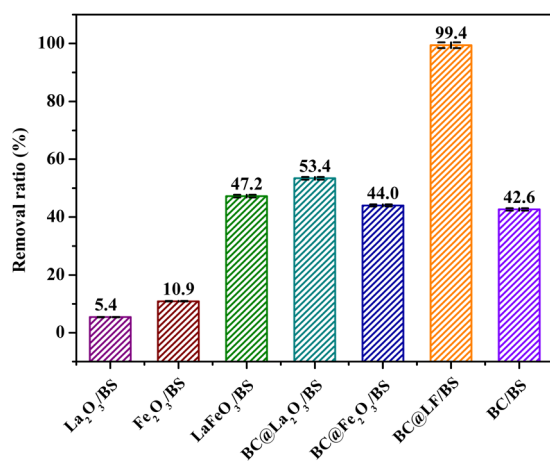

Fig. 9 Removal of MB in different systems. Experimental conditions: [MB]$_0$ = 15 mg L$^{−1}$, [BC@LF]$_0$ = [BC]$_0$ = [LaFeO$_3$]$_0$ = [La$_2$O$_3$]$_0$ = [Fe$_2$O$_3$]$_0$ = [BC@La$_2$O$_3$]$_0$ = [BC@ Fe$_2$O$_3$]$_0$ = 3 g L$^{−1}$, [BS] = 5 mM, T = 25 °C, pH$_0$ = 7.
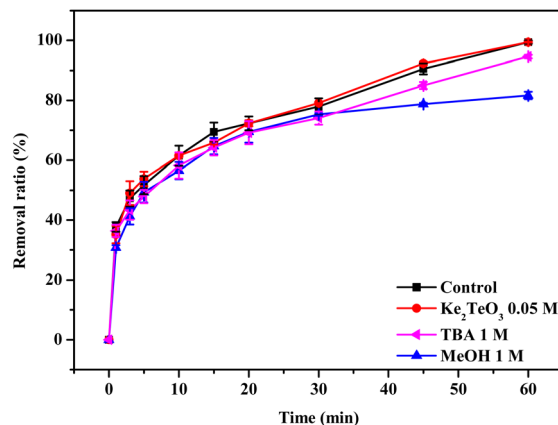
Fig. 10 Effect of scavengers on MB removal in BC@LF/BS system. Experimental conditions: [MB]$_0$ = 15 mg L$^{−1}$, [BC@LF]$_0$ = 3 g L$^{−1}$, [BS]$_0$ = 5 mM, T = 25 °C, pH$_0$ = 7.

HO$^•$ was 1900 times higher than that with SO$_4$$^{•−}$ ($k_{TBA,HO^•}$ = 7.6 × 10^8 M$^{−1}$ s$^{−1}$ vs. $k_{TBA,SO_4^{•−}}$ = 4.0 × 10^5 M$^{−1}$ s$^{−1}$),[56] hence, the introduction of TBA could selectively quench HO$^•$ in BC@LF/BS system, while MeOH could quench both SO$_4$$^{•−}$ and HO$^•$ ($k_{MeOH,HO^•}$ = 9.7 × 10^8 M$^{−1}$ s$^{−1}$ and $k_{MeOH,SO_4^{•−}}$ = 2.5 × 10^7 M$^{−1}$ s$^{−1}$).[57] However, these two alcohols could hardly quench SO$_5$$^{•−}$.[58] As shown in Fig. 9, MB removal ratio decreased from 99.4% to 95.2% in BC@LF/BS system with the addition of 1 M TBA, which might be ascribed to the quenching o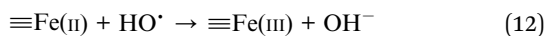f HO$^•$. However, the degradation of MB was further suppressed in the presence of 1 M MeOH. The stronger inhibition effect of MeOH on MB removal than that of TBA suggested that SO$_4$$^{•−}$ was present and played a role in MB degradation in BC@LF/BS system.

To investigate the possibility of ≡Fe(IV) degrading MB, K$_2$TeO$_3$ was introduced in BC@LF/BS system. Gupta et al.[59] reported that Te(IV) was a good stabilizing agent to stabilize oxidation states of transition metal ion in heterogeneous condition. During the reaction, Te(IV) would be complexed with ≡Fe(IV) to exclude the possibility of MB degradation by ≡Fe(IV).[60] As shown in Fig. 10, the removal of MB was hardly changed after introducing K$_2$TeO$_3$ into BC@LF/BS system, suggesting that ≡Fe(IV) might have no role in MB removal.

In conclusion, both SO$_4$$^{•−}$ and HO$^•$ participated in MB degradation in BC@LF/BS system, and SO$_5$$^{•−}$ might also be involved in MB degradation due to the incomplete inhibition of MB degradation with 1 M MeOH.

$$\equiv Fe(III) + HSO_3^- \rightarrow \equiv Fe^{III}SO_3^+ + H^+ \quad (3)$$

$$\equiv Fe^{III}SO_3^+ \rightarrow \equiv Fe(II) + SO_3^{•-} \quad (4)$$

$$SO_3^{•-} + O_2 \rightarrow SO_5^{•-} \quad (5)$$

$$SO_5^{•-} + HSO_3^- \rightarrow SO_4^{2-} + SO_4^{•-} + H^+ \quad (6)$$

$$2SO_5^{•-} \rightarrow 2SO_4^{•-} + O_2 \quad (7)$$

$$SO_4^{•-} + HSO_3^- \rightarrow SO_3^{•-} + SO_4^{2-} + H^+ \quad (8)$$

$$SO_4^{\cdot-} + OH^- \rightarrow SO_4^{2-} + HO^\cdot \qquad (9)$$

$$SO_4^{\cdot-} + H_2O \rightarrow SO_4^{2-} + HO^\cdot + H^+ \qquad (10)$$

$$HO^\cdot + HSO_3^- \rightarrow SO_3^{\cdot-} + H_2O \qquad (11)$$

$$\equiv Fe(II) + HO^\cdot \rightarrow \equiv Fe(III) + OH^- \qquad (12)$$

$$\equiv Fe(II) + SO_4^{\cdot-} \rightarrow \equiv Fe(III) + SO_4^{2-} \qquad (13)$$

$$\equiv Fe(II) + HSO_3^- \rightarrow \equiv Fe^{II}HSO_3^+ \qquad (14)$$

$$\equiv Fe^{II}HSO_3^+ + 0.25O_2 \rightarrow \equiv Fe^{III}SO_3^+ + 0.5H_2O \qquad (15)$$
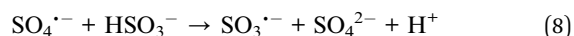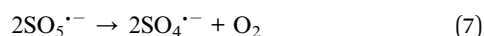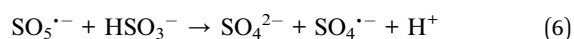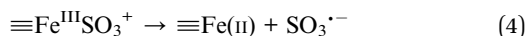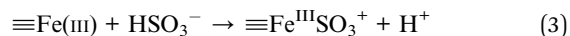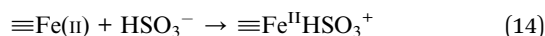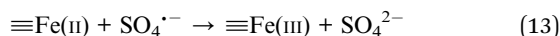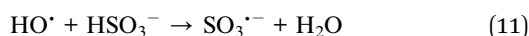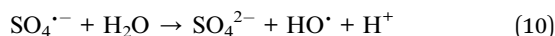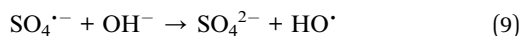
3.4. Identification of MB removal behavior in BC@LF/BS system

To further investigate the MB removal behavior in BC@LF/BS system, a comparison was made between the BC + LaFeO$_3$/BS and BC@LF/BS systems for MB removal, as shown in Fig. 11. The MB removal efficiency was 68.2% and 99.4% in BC + LaFeO$_3$/BS and BC@LF/BS systems, respectively, indicating a synergistic enhancement effect of BC@LF composite material for MB removal. Additionally, the pH variation showed a remarkable decrease in the BC@LF/BS system, whereas the BC + LaFeO$_3$/BS system exhibited only a slight decrease in pH. Considering that BS activation generates H$^+$ (eqn (2), (5), (7) and (9)), this observation suggested that the activation of BS in BC + LaFeO$_3$/BS system was limited.

To further validate this speculation, 10 mM of CA was added to the reaction solution after reaction and stirred for 30 minutes to desorb MB. The MB removal efficiency in BC + LaFeO$_3$/BS system dropped to 7.3% after desorption, while the BC@LF/BS system maintained a high removal efficiency of 96.4%. This finding supports that the MB removal in BC@LF/BS system involved simultaneous processes of adsorption and degradation, while the adsorption and degradation processes occurred separately in BC + LaFeO$_3$/BS system. Hence, the MB removal
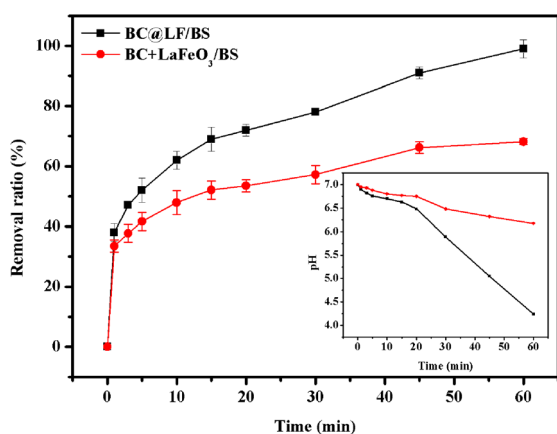
Fig. 12 Removal efficiency of MB by BC@LF/BS (a) and BC@LF adsorption (b) at different pH values. Experimental conditions: $[MB]_0 = 15$ mg L^{-1}, $[BC@LF]_0 = 3$ g L^{-1}, $[BS]_0 = 5$ mM, $T = 25$ °C.

mechanisms in BC@LF/BS and BC + LaFeO$_3$/BS systems were entirely different.

3.5. Effect of pH on MB removal

Solution pH plays an important role in the BS-based AOPs because it can significantly affect the existing form of BS and subsequent formation of free radicals.[48] Hence, to explore the impact of acidic, neutral and alkaline conditions on MB degradation in BC@LF/BS system, a wide pH range (3–11) was

Fig. 11 Removal of MB by BC@LF/BS system and BC + LaFeO$_3$/BS system. Experimental conditions: $[MB]_0 = 15$ mg L^{-1}, $[BC@LF]_0 = 3$ g L^{-1}, $[BC]_0 = 2$ g L^{-1}, $[LaFeO_3]_0 = 1$ g L^{-1}, $[BS]_0 = 5$ mM, $T = 25$ °C, pH$_0 = 7$.

Fig. 13 Recyclability test of BC@LF on BS activation for MB degradation. Experimental conditions: $[MB]_0 = 15$ mg L^{-1}, $[BC@LF]_0 = 3$ g L^{-1}, $[BS]_0 = 5$ mM, $T = 25$ °C, pH$_0 = 7$.

Table 3 EDS data of fresh and used BC@LF

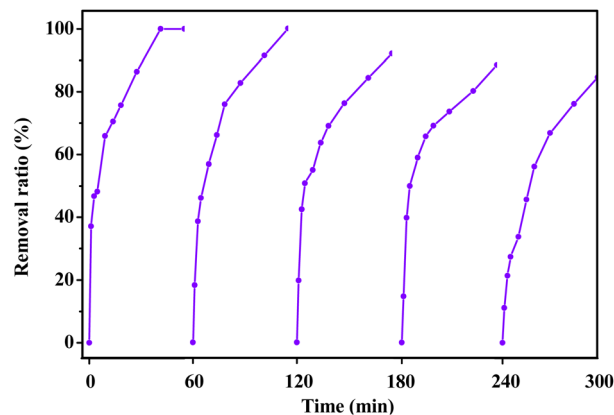| Element	Fresh BC@LF			Used BC@LF (five cycles)		
	Mass percent	Wt% sigma	Atomic percent	Mass percent	Wt% sigma	Atomic percent
C	31.01	0.41	61.33	23.41	0.30	46.12
O	17.55	0.19	26.06	28.02	0.24	41.45
Fe	13.61	0.20	5.79	16.40	0.24	6.95
La	37.83	0.31	6.82	32.17	0.30	5.48

selected, and specific initial pH values (3, 5, 7, 9, 11) were adjusted using H_2SO_4 and NaOH, as shown in Fig. 12a. The removal ratio of MB within 60 min was close to 100% at pH 3, 5 and 7, while its degradation efficiency was obviously decreased at pH 9 and 11. Interestingly, in the initial stage of the reaction (0–15 min), the removal rate of MB at alkaline conditions (pH 9 and 11) was faster than that at acidic conditions (pH 3 and 5). This might be due to the different adsorption and degradation capabilities of BC@LF at different pH values. The removal of MB by BC@LF adsorption at studied pH values was thus investigated, and the results are presented in Fig. 12b. The adsorption of MB by BC@LF increased with increasing pH. However, under alkaline conditions, OH^- could compete with MB for $SO_4^{\bullet-}$ and $HO^{\bullet}$ in BC@LF/BS system, restraining MB elimination.[61] Additionally, the ferrihydrite ($FeOH^{2+}$, $Fe_2(OH)_2^{4+}$ and $Fe(OH)_2^+$) might also be formed on the catalyst surface in alkaline conditions, which might suppress BS activation and subsequent formation of reactive radicals.[62] Therefore, in initial stage of reaction, the faster MB removal under alkaline conditions was probably due to its increased adsorption by BC@LF, while the higher MB degradation after reaction under acidic conditions might be because of its efficiently catalytic oxidation. At pH 7, high MB elimination in BC@LF/BS system in the whole reaction might be ascribed to both its excellent adsorption and catalytic degradation.

3.6. Reusability of BC@LF

To investigate the reusability of BC@LF, the recyclability test of the catalyst was performed. The used BC@LF was recyclability at the same experimental condition. As shown in Fig. 13, MB removal in BC@LF/BS system decreased from 99.9% to 84.6% after five cycles, suggesting a good reusability of BC@LF. In addition, as shown in EDS data of fresh and used BC@LF (Table 3), the element composition of BC@LF was rarely changed after reaction, which further suggested the good reusability of BC@LF. Furthermore, the leaching values of La and Fe obtained from the ICP-MS test were 0.41 mg L^{-1} and 0.48 mg L^{-1}, respectively, providing further evidence to support this inference.

3.7. Degradation of various contaminants in BC@LF/BS system

To verify the applicability of BC@LF/BS system, five typical organics including RhB, OG, DCF, SMX and OFX were chosen as the target pollutants. Their removal ratio were 94.4%, 93.1%, 90.2%, 73.1% and 94.0% in this system within 60 min,
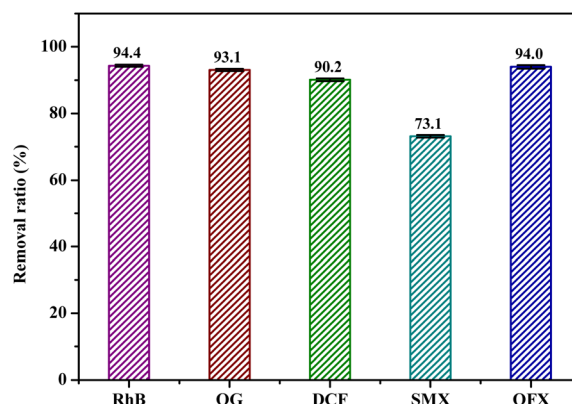

Fig. 14 Degradation of various contaminants in BC@LF/BS system. Experimental conditions: $[RhB]_0 = [OG]_0 = 15$ mg L^{-1}, $[DCF]_0 = [SMX]_0 = [OFX]_0 = 50$ μM, $[BC@LF]_0 = 3$ g L^{-1}, $[BS]_0 = 5$ mM, $T = 25$ °C, $pH_0 = 7$.

respectively, as depicted in Fig. 14. Such results indicated that BC@LF/BS system was an efficient technology for the treatment of organic pollutants.

4   Conclusion

In this study, a composite material BC@LF was synthesized using the sol–gel method with ultrasound assistance. Catalyst characterization results indicated that $LaFeO_3$ was successfully loaded on BC and $\equiv Fe(III)$ in $LaFeO_3$ was the dominant active sites for BS catalysis. Quenching experiments demonstrated that $SO_4^{\bullet-}$ and $HO^{\bullet}$ were the dominant radicals for MB degradation in BC@LF/BS system, and $SO_5^{\bullet-}$ might also play a role in MB removal. Acidic and neutral conditions were beneficial for MB removal in this system. BC@LF exhibited an excellent reusability for BS activation after five cycles. The efficient removal of RhB, OG, DCF, SMX and OFX in BC@LF/BS system indicated that this system possessed a wide applicability for the degradation of organic pollutants.

Author contributions

(1) Xiangyu Meng: investigation, writing – original draft preparation. (2) Yao Li: investigation. (3) Yiqing Liu: conceptualization, methodology, formal analysis, data curation, writing – reviewing and editing. (4) Runyu Zhou: investigation. (5) Yongsheng Fu: resources and supervision. (6) Junmin Chen: resources and supervision.

Conflicts of interest

There are no conflicts to declare.

Acknowledgements

References

1 P. M. Bulemo and I.-D. Kim, Recent advances in ABO_3 perovskites: their gas-sensing performance as resistive-type gas sensors, *J. Korean Ceram. Soc.*, 2020, **57**, 24–39.

2 C. Hao, G. Li, G. Wang, W. Chen and S. Wang, Preparation of acrylic acid modified alkalized MXene adsorbent and study on its dye adsorption performance, *Colloids Surf., A*, 2022, **632**, 127730.

3 D. Ma, H. Yi, C. Lai, X. Liu, X. Huo, Z. An, L. Li, Y. Fu, B. Li, M. Zhang, L. Qin, S. Liu and L. Yang, Critical review of advanced oxidation processes in organic wastewater treatment, *Chemosphere*, 2021, **275**, 130104.

4 U. Ushani, X. Lu, J. Wang, Z. Zhang, J. Dai, Y. Tan, S. Wang, W. Li, C. Niu, T. Cai, N. Wang and G. Zhen, Sulfate radicals-based advanced oxidation technology in various environmental remediation: A state-of-the-art review, *Chem. Eng. J.*, 2020, **402**, 126232.

5 S. Giannakis, K.-Y. A. Lin and F. Ghanbari, A review of the recent advances on the treatment of industrial wastewaters by sulfate radical-based advanced oxidation processes (SR-AOPs), *Chem. Eng. J.*, 2021, **406**, 127083.

6 H. Zhang, W. Guan, L. Zhang, X. Guan and S. Wang, Degradation of an organic dye by bisulfite catalytically activated with iron manganese oxides: The role of superoxide radicals, *ACS Omega*, 2020, **5**, 18007–18012.

7 T. Luo, Y. Peng, L. Chen, J. Li, F. Wu and D. Zhou, Metal-free electro-activated sulfite process for As(III) oxidation in water using graphite electrodes, *Environ. Sci. Technol.*, 2020, **54**, 10261–10269.

8 Z. Wang, D. Shen, F. Shen, C. Wu and S. Gu, Kinetics, equilibrium and thermodynamics studies on biosorption of Rhodamine B from aqueous solution by earthworm manure derived biochar, *Int. Biodeterior. Biodegrad.*, 2017, **120**, 104–114.

9 S. Duan, P. Hou, X. Yuan, M. Habuda Stanić, Z. Qiang and H. Dong, Homogeneous activation of bisulfite by transition metals for micro-pollutant degradation: Mn(VII) versus Cr(VI), *Chem. Eng. J.*, 2020, **394**, 124814.

10 H. Wang, S. Wang, Y. Liu, Y. Fu, P. Wu and G. Zhou, Degradation of diclofenac by Fe(II)-activated bisulfite: Kinetics, mechanism and transformation products, *Chemosphere*, 2019, **237**, 124518–124527.

11 R. Dou, H. Cheng, J. Ma, Y. Qin, Y. Kong and S. Komarneni, Catalytic degradation of methylene blue through activation of bisulfite with CoO nanoparticles, *Sep. Purif. Technol.*, 2020, **239**, 116561–116568.

12 C. Guan, Q. Guo, Z. Wang, X. Wei, B. Han, X. Luo, H. Pan and J. Jiang, Bisulfite activated permanganate for oxidative water decontamination, *Water Res.*, 2022, **216**, 118331.

13 X. Yu, X. Jin, H. Liu, Y. Yu, J. Tang, R. Zhou, A. Yin, J. Sun and L. Zhu, Enhanced degradation of atrazine through UV/bisulfite: Mechanism, reaction pathways and toxicological analysis, *Sci. Total Environ.*, 2023, **856**, 159157.

14 H. Liu, C. Wang and G. Wang, Photocatalytic advanced oxidation processes for water treatment: Recent advances and perspective, *Chem.–Asian J.*, 2020, **15**, 3239–3253.

15 M. Cheng, Y. Liu, D. Huang, C. Lai, G. Zeng, J. Huang, Z. Liu, C. Zhang, C. Zhou, L. Qin, W. Xiong, H. Yi and Y. Yang, Prussian blue analogue derived magnetic Cu-Fe oxide as a recyclable photo-Fenton catalyst for the efficient removal of sulfamethazine at near neutral pH values, *Chem. Eng. J.*, 2019, **362**, 865–876.

16 Z. Wang, J. Li, W. Song, R. Ma, J. Yang, X. Zhang, F. Huang and W. Dong, Rapid degradation of atrazine by a novel advanced oxidation process of bisulfite/chlorine dioxide: Efficiency, mechanism, pathway, *Chem. Eng. J.*, 2022, **445**, 136558.

17 H. Zhao, L. Qian, X. Guan, D. Wu and G. Zhao, Continuous Bulk FeCuC Aerogel with ultradispersed metal nanoparticles: An efficient 3D heterogeneous electro-Fenton cathode over a wide range of pH 3–9, *Environ. Sci. Technol.*, 2016, **50**, 5225–5233.

18 M. Mohseni, W. Zängler, K. Demeestere, G. Du Laing, S. Bhandari, A. K. Mechler, S. Yüce, R. G. Keller and M. Wessling, One-pot synthesized, Fe-incorporated self-standing carbons with a hierarchical porosity remove carbamazepine and sulfamethoxazole through heterogeneous electro-Fenton, *Chem. Eng. J.*, 2022, **446**, 137006.

19 Q. Ji, L. Bi, J. Zhang, H. Cao and X. S. Zhao, The role of oxygen vacancies of ABO_3 perovskite oxides in the oxygen reduction reaction, *Energy Environ. Sci.*, 2020, **13**, 1408–1428.

20 H. Zhang, S. Cheng, B. Li, X. Cheng and Q. Cheng, Fabrication of magnetic $Co/BiFeO_3$ composite and its advanced treatment of pharmaceutical waste water by activation of peroxysulphate, *Sep. Purif. Technol.*, 2018, **202**, 242–247.

21 T. Soltani, A. Tayyebi and B.-K. Lee, Quick and enhanced degradation of bisphenol A by activation of potassium peroxymonosulfate to SO_4^- with Mn-doped $BiFeO_3$ nanoparticles as a heterogeneous Fenton-like catalyst, *Appl. Surf. Sci.*, 2018, **441**, 853–861.

22 S. G. Babu, P. Aparna, G. Satishkumar, M. Ashokkumar and B. Neppolian, Ultrasound-assisted mineralization of organic contaminants using a recyclable $LaFeO_3$ and Fe^{3+}/persulfate Fenton-like system, *Ultrason. Sonochem.*, 2017, **34**, 924–930.

23 Y. Nie, L. Zhang, Y. Li and C. Hu, Enhanced Fenton-like degradation of refractory organic compounds by surface complex formation of $LaFeO_3$ and H_2O_2, *J. Hazard. Mater.*, 2015, **294**, 195–200.

24 Y. Rao, Y. Zhang, F. Han, H. Guo, Y. Huang, R. Li, F. Qi and J. Ma, Heterogeneous activation of peroxymonosulfate by LaFeO$_3$ for diclofenac degradation: DFT-assisted mechanistic study and degradation pathways, *Chem. Eng. J.*, 2018, **352**, 601–611.

25 Y. Zhou, B. Gao, A. R. Zimmerman, H. Chen, M. Zhang and X. Cao, Biochar-supported zerovalent iron for removal of various contaminants from aqueous solutions, *Bioresour. Technol.*, 2014, **152**, 538–542.

26 J. Xu, X. Zhang, C. Sun, H. He, Y. Dai, S. Yang, Y. Lin, X. Zhan, Q. Li and Y. Zhou, Catalytic degradation of diatrizoate by persulfate activation with peanut shell biochar-supported nano zero-valent iron in aqueous solution, *Int. J. Environ. Res. Public Health*, 2018, **15**, 1937–1955.

27 S. Yang, X. Yang, X. Shao, R. Niu and L. Wang, Activated carbon catalyzed persulfate oxidation of Azo dye acid orange 7 at ambient temperature, *J. Hazard. Mater.*, 2011, **186**, 659–666.

28 Z. Shen, D. Hou, B. Zhao, W. Xu, Y. S. Ok, N. S. Bolan and D. S. Alessi, Stability of heavy metals in soil washing residue with and without biochar addition under accelerated ageing, *Sci. Total Environ.*, 2018, **619–620**, 185–193.

29 B. Yang, Y. Feng, Y. Yu, S. He, H. Liu, L. Xue and L. Yang, Lanthanum ferrite nanoparticles modification onto biochar: derivation from four different methods and high performance for phosphate adsorption, *Environ. Sci. Pollut. Res. Int.*, 2019, **26**, 22010–22020.

30 X. Chen, M. Zhang, H. Qin, J. Zhou, Q. Shen, K. Wang, W. Chen, M. Liu and N. Li, Synergy effect between adsorption and heterogeneous photo-Fenton-like catalysis on LaFeO$_3$/lignin-biochar composites for high efficiency degradation of ofloxacin under visible light, *Sep. Purif. Technol.*, 2022, **280**, 119751–119764.

31 R. Dou, H. Cheng, J. Ma, Y. Qin, Y. Kong and S. Komarneni, Catalytic degradation of methylene blue through activation of bisulfite with CoO nanoparticles, *Sep. Purif. Technol.*, 2020, **239**, 116561.

32 B. Guo, J. Ma, Y. Shi, K. Zheng, M. Wu, G. Ren and S. Komarneni, Co$_3$O$_4$/CoO ceramic catalyst: Bisulfite assisted catalytic degradation of methylene blue, *Ceram. Interfaces*, 2021, **47**, 27617–27623.

33 Z. Hou, J. Ma, C. Fan, M. Peng and S. Komarneni, Iron activated sodium bisulfite enhances generation of Mn^{3+}pecies through the MnO$_2$/bisulfite catalytic process, *Ceram. Interfaces*, 2019, **45**, 892–898.

34 Y. Li, X. Meng, Y. Pang, C. Zhao, D. Peng, Y. Wei and B. Xiang, Activation of bisulfite by LaFeO$_3$ loaded on red mud for degradation of organic dye, *R. Soc. Open Sci.*, 2022, **9**, 220466.

35 J. Yan, W. Liu, R. Sun, S. Jiang, S. Wang and L. Shen, Chemical looping catalytic gasification of biomass over active LaNiFe$_1$-O$_3$ perovskites as functional oxygen carriers, Chinese, *J. Chem. Eng.*, 2021, **36**, 146–156.

36 H. Shen, T. Xue, Y. Wang, G. Cao, Y. Lu and G. Fang, Photocatalytic property of perovskite LaFeO$_3$ synthesized by sol-gel process and vacuum microwave calcination, *Mater. Res. Bull.*, 2016, **84**, 15–24.

37 S. Orimo, T. Matsushima, H. Fujii, T. Fukunaga and G. Majer, Hydrogen desorption property of mechanically prepared nanostructured graphite, *J. Appl. Phys.*, 2001, **90**, 1545–1549.

38 H. Zhou, S. Zhu, M. Hibino, I. Honma and M. Ichihara, Lithium storage in ordered mesoporous carbon (CMK-3) with high reversible specific energy capacity and good cycling performance, *Adv. Mater.*, 2003, **15**, 2107–2111.

39 S. Zhuo, H. Ren, G. Cao, G. Xie, D. Xing, N. Ren and B. Liu, Highly efficient activation of persulfate by encapsulated nano-Fe^0 biochar for acetaminophen degradation: Rich electron environment and dominant effect of superoxide radical, *Chem. Eng. J.*, 2022, **440**, 135947.

40 M. Thommes, K. Kaneko, A. V. Neimark, J. P. Olivier, F. Rodriguez-Reinoso, J. Rouquerol and K. S. W. Sing, Physisorption of gases, with special reference to the evaluation of surface area and pore size distribution (IUPAC Technical Report), *Pure Appl. Chem.*, 2015, **87**, 1051–1069.

41 D. H. E. K. S. W. Sing, R. A. W. Haul, L. Moscou, R. A. Pieroti, J. Rouquerol and T. Siemieniewska, Reporting physisorption data for gas/solid systems, *Pure Appl. Chem.*, 1985, **57**, 603–619.

42 M. D. Huff, S. Kumar and J. W. Lee, Comparative analysis of pinewood, peanut shell, and bamboo biomass derived biochars produced via hydrothermal conversion and pyrolysis, *J. Environ. Manage.*, 2014, **146**, 303–308.

43 D. K. Ojha, V. S. P. Kumar and R. Vinu, Analytical pyrolysis of bagasse and groundnut shell briquettes: Kinetics and pyrolysate composition studies, *Bioresour. Technol. Rep.*, 2021, **15**, 100784.

44 B. Chen, Z. Chen and S. Lv, A novel magnetic biochar efficiently sorbs organic pollutants and phosphate, *Bioresour. Technol.*, 2011, **102**, 716–723.

45 J. Meng, X. Feng, Z. Dai, X. Liu, J. Wu and J. Xu, Adsorption characteristics of Cu(II) from aqueous solution onto biochar derived from swine manure, *Environ. Sci. Pollut. Res. Int.*, 2014, **21**, 7035–7046.

46 P. V. Gosavi and R. B. Biniwale, Pure phase LaFeO$_3$ perovskite with improved surface area synthesized using different routes and its characterization, *Mater. Chem. Phys.*, 2010, **119**, 324–329.

47 G. Sierra Gallego, N. Marín Alzate and O. Arnache, A novel LaFeO$_3$−$_X$N$_X$ oxynitride. Synthesis and characterization, *J. Alloys Compd.*, 2013, **549**, 163–169.

48 P. Tang, Y. Tong, H. Chen, F. Cao and G. Pan, Microwave-assisted synthesis of nanoparticulate perovskite LaFeO$_3$ as a high active visible-light photocatalyst, *Curr. Appl. Phys.*, 2013, **13**, 340–343.

49 S. Phokha, S. Pinitsoontorn, S. Rujirawat and S. Maensiri, Polymerized complex synthesis and effect of Ti dopant on magnetic properties of LaFeO$_3$ nanoparticles, *J. Nanosci. Nanotechnol.*, 2015, **15**, 9171–9177.

50 V. M. Gaikwad, J. R. Sheikh and S. A. Acharya, Investigation of photocatalytic and dielectric behavior of LaFeO$_3$

nanoparticles prepared by microwave-assisted sol-gel combustion route, *J. Sol-Gel Sci. Technol.*, 2015, **76**, 27–35.

51 K. M. Parida, K. H. Reddy, S. Martha, D. P. Das and N. Biswal, Fabrication of nanocrystalline LaFeO₃: An efficient sol-gel auto-combustion assisted visible light responsive photocatalyst for water decomposition, *Int. J. Hydrogen Energy*, 2010, **35**, 12161–12168.

52 S. Wang, G. Wang, Y. Fu, H. Wang and Y. Liu, A simple Fe^{3+}/bisulfite system for rapid degradation of sulfamethoxazole, *RSC Adv.*, 2020, **10**, 30162–30168.

53 Q. Wang, C. Luo, X. Li, H. Ding, C. Shen, D. Cao and L. Zhang, Development of LaFeO₃ modified with potassium as catalyst for coal char CO_2 gasification, *J. CO₂ Util.*, 2019, **32**, 163–169.

54 Y. Qin, H. Tian and L. Zhang, Study on the correlation of delectron configuration and catalytic oxidation activity of LaMO₃ compounds, *Acta Chim. Sin.*, 1993, **51**, 319–324.

55 D. Zhou, Y. Yuan, S. Yang, H. Gao and L. Chen, Roles of oxysulfur radicals in the oxidation of acid orange 7 in the Fe(III)–sulfite system, *J. Sulfur Chem.*, 2015, **36**, 373–384.

56 P. Neta, R. E. Huie and A. B. Ross, Rate constants for reactions of inorganic radicals in aqueous solution, *J. Phys. Chem. Ref. Data*, 1988, **17**, 1027–1284.

57 G. P. Anipsitakis and D. D. Dionysiou, Radical generation by the interaction of transition metals with common oxidants, *Environ. Sci. Technol.*, 2004, **38**, 3705–3712.

58 S. Liu, Y. Fu, G. Wang and Y. Liu, Degradation of sulfamethoxazole by UV/sulfite in presence of oxygen: Efficiency, influence factors and mechanism, *Sep. Purif. Technol.*, 2021, **268**, 118709.

59 C. Gupta, Synthesis, Characterization, and X-ray Diffraction Studies of Co(II), Ni(II), and Cu(II) Tellurite (TeO_3^{2-}) Complexes with Nicotinic Acid, *Synth. React. Inorg. Met.-Org. Chem.*, 2010, **40**, 5–11.

60 W. Levason, The coordination chemistry of periodate and tellurate ligands, *Coord. Chem. Rev.*, 1997, **161**, 33–79.

61 Z. Zhang, J. Li, Y. Zhao, T. Wen, T. Zhang and S. Song, Synthetic Fe-rich nontronite as a novel activator of bisulfite for the efficient removal of tetracycline, *J. Environ. Manage.*, 2022, **302**, 114002.

62 J. Zhao, F. Wu, Q. He and Y. Feng, Enhanced degradation of amiloride over Bi2FeNbO7/bisulfite process: Key factors and mechanism, *Chemosphere*, 2022, **300**, 134573.